

Hydrodynamic interactions between two spheres at contact

M. L. Ekiel-Jezewska,^{1,2,*} F. Feuillebois,¹ N. Lecoq,³ K. Masmoudi,³ R. Anthore,³ F. Bostel,³ and E. Wajnryb²

¹*Physique Thermique, PMMH ESPCI, 10 rue Vauquelin, 75231 Paris Cedex 05, France*

²*IPPT, Polish Academy of Sciences, Świątokrzyska 21, 00-049 Warsaw, Poland*

³*Université de Rouen, UMR 6634 CNRS, Place E. Blondel, 76821 Mont Saint Aignan Cedex, France*

(Received 26 August 1998)

We develop a model of contact interactions between two spherical particles immersed in a viscous fluid, under a very low Reynolds number. This model allows us to interpret results of our experiment, in which the settling motion of a ball in the vicinity of another fixed sphere is accurately measured with laser interferometry. Due to the symmetry of the experimental setup and the reversibility of the Stokes equations describing the fluid flow, the trajectory and velocity of the moving sphere center are expected to exhibit symmetry with respect to reflection in the horizontal plane containing the fixed sphere center. However, no such symmetry is observed if the particles “touch” each other. Our model accounts for symmetry breaking by the contact friction between surfaces—such a force appears only when the moving sphere center is above the horizontal plane containing the center of the fixed particle. The model predicts two intervals of motion, at contact: pure rolling and rolling with slip. The existence of both types of motion, with a sharp transition from one to another, has been verified experimentally. [S1063-651X(99)05303-9]

PACS number(s): 47.15.Gf, 47.15.Pn, 46.55.+d, 81.40.Pq

I. INTRODUCTION

The title of this paper seems to contradict the standard Jeffrey-Onishi theory of low-Reynolds-number hydrodynamic interactions between two spheres, according to which friction forces slow down the motion of particles approaching each other, preventing them from contact [1–5]. However, for small separations between particle surfaces, additional effects may become important [6–9]. A particle with a rough surface is no longer perfectly spherical, and the standard lubrication theory (i.e., theory of the hydrodynamic interactions for a very small gap between particle surfaces) needs to be modified to account for the real surface shape.

The goal of this paper is to develop a simple model of combined hydrodynamic and contact interactions between two spheres, and apply it to account for our experimental data. Our system consists of two spheres of approximately equal size immersed in a viscous oil: one of them is fixed, and another one moves freely nearby, due to gravity. The particle instantaneous velocity is measured during its motion. To determine the vertical component we have applied an accurate interferometric technique developed earlier [10]. The method used to determine the particle horizontal velocity and its trajectory is based on a coupling of the interferometric setup with encoders [11,12], and it will be presented elsewhere.

Our model contains essentially the same physics of contact as the roll and slip model of Davis [7]. However, Davis introduced hydrodynamic interactions with contact friction for a different system, in which a heavy sphere sedimenting through a dilute suspension of neutrally buoyant particles interacts pairwise with a *mobile* sphere. Therefore his equations and calculations differ from ours. The roll and slip model from Ref. [7] was later checked to agree with an ex-

periment based on video recording and computer image analysis [9]. The interferometric technique [10–12] used in our experiments has a significantly higher accuracy than the system used in Ref. [9]. Such an accurate tool allows us to test more precisely the existence of pure rolling, and rolling with slip, at contact. It would also allow one to further develop the simple physical model presented here; however, this is beyond the scope of this paper. Here we concentrate on presenting basic concepts of the model, and on describing how the improvement of the model and the redesign of the experiment were interrelated.

In Sec. II we introduce the hydrodynamic interactions, and explain how its standard theoretical description leads to the expectation of symmetries of velocity plots and trajectories. In Sec. III we present how the symmetry is broken in the experimental data. In Sec. IV we explain how the contact friction can be combined with hydrodynamic interactions. We present the basic structure of the model and the mechanism by which it causes the symmetry breaking. In Sec. V we specify the quantities provided by the experiment and their accuracy, explaining the method of measurement. This information is used in Sec. VI to write down the model equations in a form well fitted for later comparison with the experiment: that is, to benefit from the measurement accuracy. In Sec. VII we present more detailed information about the experiment, which enables us to redesign the model and check its validity limits in Sec. VIII. Interpretation of the experimental data with the model is finally performed in Sec. IX, leading to the conclusions presented in Sec. X.

II. HYDRODYNAMIC INTERACTIONS BETWEEN TWO SPHERES

A. Formulation of the problem

Consider two spheres of equal radii in low-Reynolds-number incompressible fluid flow. The fluid is described by its velocity \mathbf{v} and its modified pressure p , satisfying the Stokes equations

*Electronic address: mekiel@ippt.gov.pl

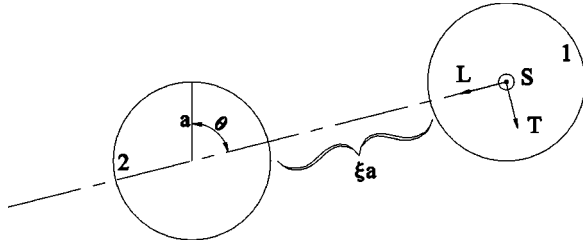


FIG. 1. Relative configuration of spheres: the notation.

$$\eta \nabla^2 \mathbf{v} - \nabla p = \mathbf{0}, \quad (1)$$

$$\nabla \cdot \mathbf{v} = 0, \quad (2)$$

with the fluid velocity vanishing at infinity and the stick boundary conditions at the sphere surfaces B_α , $\alpha = 1, 2$:

$$\mathbf{v}|_\infty = \mathbf{0}, \quad (3)$$

$$\mathbf{v}|_{B_\alpha} = \mathbf{U}_\alpha + \mathbf{\Omega}_\alpha \times (\mathbf{r} - \mathbf{r}_\alpha), \quad (4)$$

where \mathbf{r} is any point at the surface B_α , \mathbf{r}_α is the α th sphere center, and \mathbf{U}_α and $\mathbf{\Omega}_\alpha$ are the α th particle translational and rotational velocities [13].

Within the approximation of negligible fluid and particle inertia, the external forces \mathbf{F}_α and torques \mathbf{T}_α acting on the particles are balanced by the corresponding hydrodynamic forces \mathbf{H}_α and hydrodynamic torques \mathbf{Q}_α exerted on them by the fluid. The forces and the torques are linearly related to the particle velocities by the friction matrix $\vec{\zeta}$, which depends on the distance between both particles, and which is calculated according to the procedure developed in Ref. [5]:

$$\begin{pmatrix} \mathbf{F}_1 \\ \mathbf{T}_1 \\ \mathbf{F}_2 \\ \mathbf{T}_2 \end{pmatrix} = \vec{\zeta} \begin{pmatrix} \mathbf{U}_1 \\ \mathbf{\Omega}_1 \\ \mathbf{U}_2 \\ \mathbf{\Omega}_2 \end{pmatrix}. \quad (5)$$

In our system sphere 2 is fixed; therefore, its translational and rotational velocities vanish. Sphere 1 moves freely, so the external force and the external torque acting on it are given. We want to solve Eq. (5) to obtain the translational velocity of the first particle \mathbf{U}_1 , and compare it with the experiment:

$$\text{given: } \mathbf{U}_2 = \mathbf{\Omega}_2 = \mathbf{0}, \quad (6)$$

$$\mathbf{F}_1, \mathbf{T}_1; \quad (7)$$

$$\text{what is: } \mathbf{U}_1? \quad (8)$$

We will follow the notation presented in Fig. 1, using two coordinate frames: LTS (marked in Fig. 1) or xzS ; z is vertical pointing up, and x is horizontal pointing right.

B. Symmetries

The Stokes equations are invariant under time reversal and under reflection in a plane. Therefore, the moving particle velocity vector is symmetric under any of those trans-

formations or their combination, if the boundary conditions on both fixed and moving particle surfaces display the corresponding symmetry.

The boundary conditions on the fixed sphere (6) are symmetric under reflection in any plane containing the fixed sphere center, as well as under time reversal. The boundary conditions on the moving sphere are given indirectly through the external forces, and their symmetries are to be analyzed by the corresponding symmetries of the external forces.

Theorem 1. If the external forces and torques acting on the moving particle are symmetric with respect to reflection in the vertical plane containing both sphere centers, then the particle motion (both translational and rotational) is restricted to this plane:

$$\Omega_{1L} = \Omega_{1T} = U_{1S} = 0. \quad (9)$$

Theorem 2. If the external forces and torques acting on the moving particle are symmetric with respect to time reversal superposed with reflection in the horizontal plane $z = 0$, containing the fixed sphere center, then the particle velocity is also symmetric under this transformation, which leads to the following symmetries of velocity components and the trajectory with respect to $z \rightarrow -z$:

$$U_{1x}(z) = -U_{1x}(-z), \quad (10)$$

$$U_{1z}(z) = U_{1z}(-z), \quad (11)$$

$$x(z) = x(-z). \quad (12)$$

C. Separated spheres

For separated particles the external force and torque acting on sphere 1 are due entirely to gravity:

$$\mathbf{F}_1 = \mathbf{G}, \quad (13)$$

$$\mathbf{T}_1 = \mathbf{0}. \quad (14)$$

Since p is the *modified* pressure, then the gravitational force \mathbf{G} is given as

$$\mathbf{G} = \frac{4}{3} \pi a^3 (\tilde{\rho} - \rho) \mathbf{g}, \quad (15)$$

where \mathbf{g} is the gravitational acceleration, a is the particle radius, $\tilde{\rho}$ is the particle density, and ρ is the fluid density.

Within the approximation of negligible fluid and particle inertia, \mathbf{G} is balanced by the hydrodynamic force \mathbf{H} exerted by the fluid. For any configuration of particles these forces are vertical, as shown in Fig. 5(B) in Sec. IV A; therefore, reflection in the horizontal plane containing the fixed sphere center leads to the same forces and torques as those characteristic for the time reversed motion. Therefore Eqs. (10)–(12) hold: trajectories and vertical velocity plots are symmetric, and horizontal velocity plots are antisymmetric functions of z .

In addition, the vertical plane containing both sphere centers is the symmetry plane of the system. Therefore, according to Eq. (9), the motion is restricted to this plane.

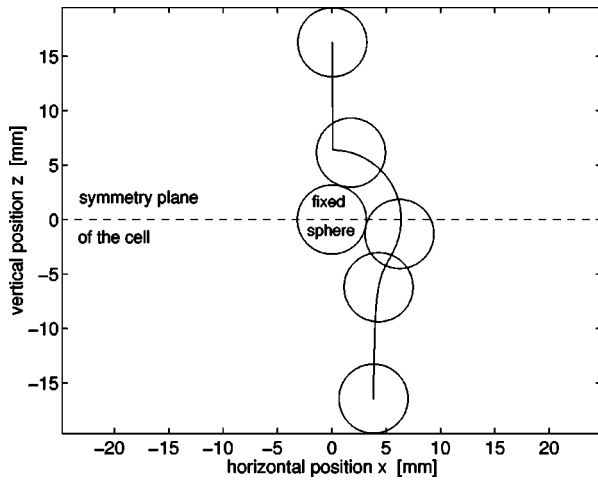


FIG. 2. A trajectory of the moving sphere center.

III. EXPERIMENTAL SYMMETRY BREAKING

In the experiment, conditions (6) and (7) are satisfied—sphere 2 is fixed, and sphere 1 moves freely from above, initially being at a distance x_0 from the vertical line including the fixed sphere center. The motion of the sphere is investigated while it passes by the fixed sphere, until the vertical distance between both particles becomes approximately the same as initially. The details of the measurement technique and the setup are presented in Secs. V and VII.

The symmetry under reflection in the vertical plane containing the fixed sphere center is observed. That is, each experimental trajectory is located in such a vertical plane. Therefore, on the plots horizontal, positions and velocities of the moving sphere are marked by only one coordinate x , measured within this plane.

The symmetry under time reversal superposed with reflection in the horizontal plane described in Sec. II B is observed in the experiment only for trajectories with x_0 larger than a certain critical value. For smaller values of x_0 there is no such a symmetry. Experimental results for a nonsymmetric single trajectory are given in Figs. 2–4.

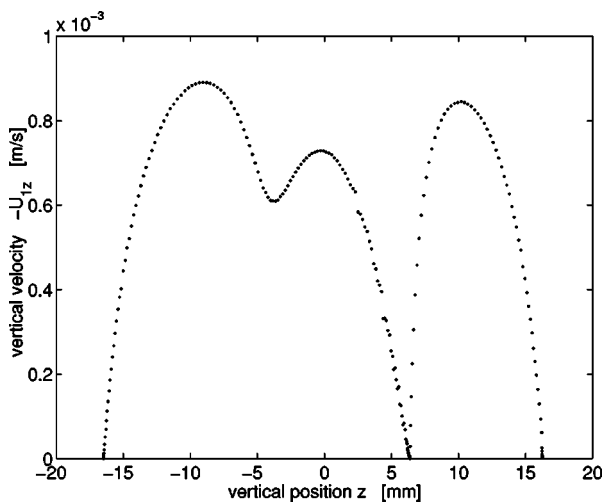


FIG. 3. Vertical velocity of the moving sphere center.

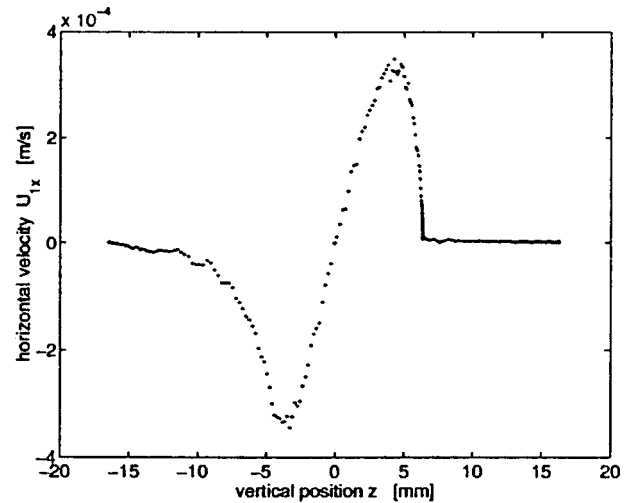


FIG. 4. Horizontal velocity of the moving sphere center.

IV. CONSTRUCTING A MODEL OF HYDRODYNAMIC AND CONTACT INTERACTIONS

A. Balance of forces and torques on spheres at contact

We assume that at contact the total external force F_1 acting on the moving sphere 1 is a superposition of the gravity force G and a contact force, consisting of a reaction of the fixed sphere P normal to its surface and a tangential solid friction force R , giving rise to a torque T_1 :

$$F_1 = G + P + R, \quad (16)$$

$$T_1 = a \times R, \quad (17)$$

where a is a vector joining the center of sphere 1 to the contact point. Since the fluid and the particle inertia are neglected, F_1 and T_1 are balanced by the hydrodynamic force H and the hydrodynamic torque Q exerted by the fluid. The forces are shown schematically in Fig. 5—all of them are in

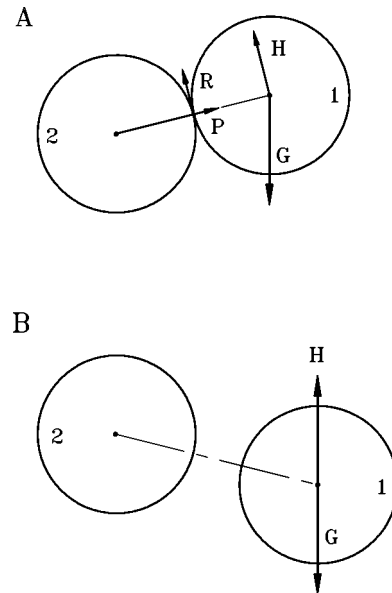


FIG. 5. Balance of forces on particle 1 (A) in contact with particle 2, and (B) separated from particle 2.

the plane of the graph, i.e., the plane xz .

As in Sec. II C, the forces and torques are symmetric under reflection in the vertical plane passing through the sphere centers, and therefore the motion is restricted to this plane. However, in contrast to Sec. II C, the forces and torques are no longer symmetric with respect to time reversal superposed with reflection in the horizontal plane $z=0$ (i.e., the plane passing through the fixed sphere center)—compare Figs. 5(A) and 5(B). Friction [as in Fig. 5(A)] appears if the gravity force pushes the moving sphere toward the fixed one—that is, if the moving particle is *above* this horizontal plane. However, friction is absent if the moving sphere is *below* this plane [cf. Fig. 5(B)]. As a result, trajectories and velocities are expected to be nonsymmetric with respect to $z \rightarrow -z$. This result is general: it is valid whatever the contact force components R and P .

B. Physical model for contact forces

To develop the model further, we need to impose two conditions specifying the contact force, i.e., its tangential and normal components P and R . First, to make the model as simple as possible, we assume that the distance between surfaces at contact does not change significantly during the motion:

$$\xi \approx \xi_m = \text{const.} \quad (18)$$

This means there is no motion along the line of sphere centers:

$$U_{1L} = 0. \quad (19)$$

This is an *ad hoc* assumption which can be refined later.

Next, we follow the standard solid friction theory [14,15] to discriminate between two generic types of motion: pure rolling, and rolling with slip. In general, the motion of bodies at contact is characterized by the ratio of the tangential to the normal forces transmitted from one surface to another, namely, by the ratio of the friction force R to the normal force pressing the bodies together P [14,15]. Suppose that this ratio increases from zero with increase of a certain control parameter (e.g., the angle θ specified in Fig. 1). First we will observe pure rolling (no sliding),

$$-a\Omega_{1S} = U_{1T}, \quad (20)$$

until a certain critical value $R/P = \mu_s$, called the static friction coefficient. At this point slip starts in addition to rolling, and R/P sharply decreases, adjusting to satisfy Amontons's law [15,16]

$$R = \mu_k P, \quad (21)$$

where μ_k is a constant, called the kinetic friction coefficient; μ_k is always smaller than μ_s . Typical values of both friction coefficients for well-lubricated metal-nonmetal contacts are about 0.05–0.12 [14].

C. Concluding the model

If the moving particle does not touch the fixed sphere during any part of its motion, then it interacts only hydrodynamically. If the particle starts close enough to the vertical

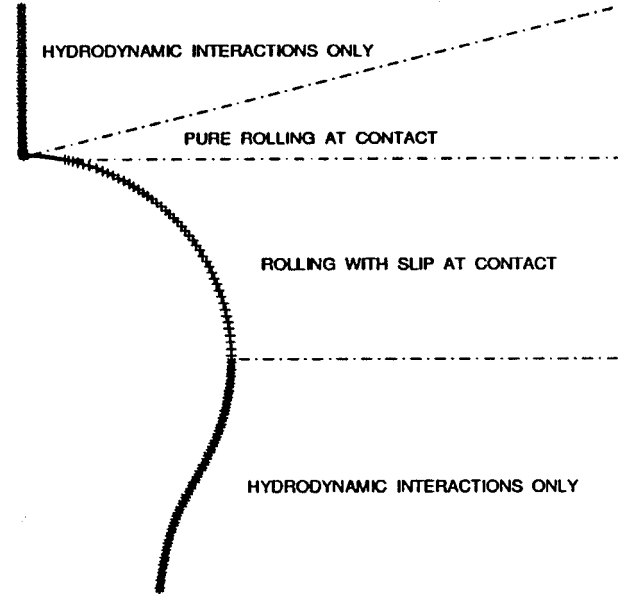


FIG. 6. Characteristic intervals of motion (for the trajectory from Fig. 2).

line containing the fixed sphere center, then for small angles θ its motion is due to hydrodynamic interactions only, but at a certain value θ_0 contact interactions with the fixed sphere become important. We assume that at contact, i.e., for θ between θ_0 and $\pi/2$, the distance ξ_m between surfaces does not change during the motion. If $\theta_0 < \theta_s$, then the pure rolling motion takes place for angles θ between θ_0 and θ_s . Rolling with slip occurs for angles θ larger than θ_0 and θ_s , but smaller than $\pi/2$. For $\theta > \pi/2$ there is no more contact, and the interactions are only through the fluid. Characteristic intervals of motion for a typical trajectory with a long contact part (the same one as those displayed in Fig. 2) are shown in Fig. 6.

According to the model, the approaching particle contacts the fixed one after a *finite* period, evaluated as the time it would take for the ideally smooth sphere to reach such a distance from the fixed (also ideally smooth) sphere, which is of the order of the roughness of the real spheres.

V. METHOD OF MEASUREMENT

Both vertical and horizontal components of the sphere motion have been investigated, but each of them with a dif-

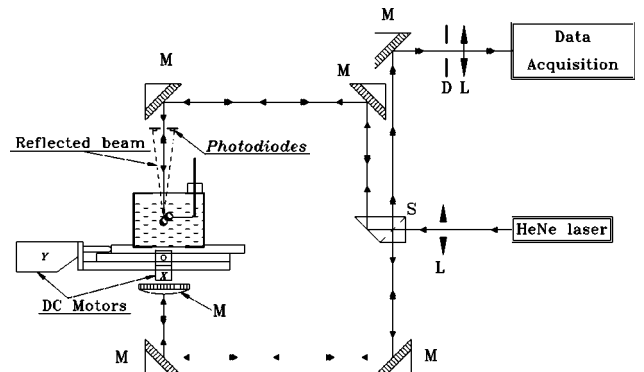


FIG. 7. Sketch of the optical interferometry setup. M , mirrors; L , lenses; S , separator; D , diaphragm.

ferent measurement technique and a different accuracy. A sketch of the experimental interferometry setup is presented in Fig. 7.

A. Vertical motion

A laser interferometer has been used to measure with high accuracy the vertical velocity and the vertical displacement of a spherical particle moving in a viscous fluid, using the technique described in Ref. [10]. The beam of a He-Ne laser is divided by a beam splitter into two beams having roughly the same power. The two beams follow symmetrical paths with the aid of mirrors. The upper beam is reflected back by the particle in motion, the lower one by a reference mirror. The two reflected beams are then superimposed to form interference fringes. The displacement of the particle results in a shifting of the interference fringes which appear as concentric clear and dark rings. Shifting from a dark fringe to the next clear fringe (or conversely) corresponds to a displacement $\Delta z = \lambda/4n$, where n is the refraction index of the liquid for the given wavelength $\lambda = 632.8$ nm; $n = 1.404$ for the silicon oil. The typical sensitivity on the measured vertical displacement is of the order of 100 nm.

The interferometric signal is then processed as follows. The times at which the signal reaches successive extremes are calculated first. The difference between such times is the elapsed time interval Δt for the particle to move a distance Δz . The frequency is $f = 1/2\Delta t$, and the particle vertical velocity is then calculated as $v_z = 2\Delta z f = \lambda f/2n$.

B. Horizontal motion

The moving particle has to stay in the vertical laser beam if the interference fringes are to be observed at each time step. However, when it moves around the fixed sphere, a horizontal component of motion is added to the vertical one. To compensate for this displacement, the whole cell is driven in such a direction that the moving sphere stays in the laser beam.

The measurements of the horizontal relative motion of the spheres are performed with a detector (a system of photodiodes), using the laser beam reflected back by the particle in motion. A horizontal displacement of the sphere is characterized by an unbalance in intensity measured by four photodiodes of the detecting system. We have checked that the intensity difference given by the photodiodes depends linearly on Δx , the horizontal displacement of the particle, if $\Delta x \leq 100$ μm . When a difference in intensity is measured, a computer performs data acquisition and calculates corrections in position (taking into account that the response of the photodiodes varies with the vertical position of the sphere). Then the corresponding command sets are sent to two direct current motors (dc motors) with high resolution shaft-mounted encoders, which drive the whole cell to compensate for the horizontal motion of the particle.

The error of the horizontal displacement is due to several factors of this complex measurement system. It can be estimated [12] as about 20 μm —the order of fluctuations of the particle horizontal position (as it has been already mentioned, the sphere is adjusted to stay at the horizontal position determined by the laser beam).

C. Resulting data

For each trial the experiment gives at successive times: vertical velocities (very accurately) and horizontal positions. This basic information allows one to calculate other characteristic parameters of the motion. In particular, horizontal velocities are deduced from horizontal displacements measured in real time, and vertical positions from vertical velocities. The trajectory of the moving particle is reconstructed at the end of each trial.

VI. CALCULATING THE MODEL OF HYDRODYNAMIC AND CONTACT INTERACTIONS

A. Quantities to be compared with experiment

In this section we use the coordinate system x , z , and S , and the notation as in Fig. 1. The measurements along the vertical direction z are significantly more accurate than those along the horizontal direction x , as explained in Sec. V. Therefore, in our model we evaluate vertical and horizontal components of the particle velocity separately, as functions of the vertical position: $U_{1z}(z)$ and $U_{1x}(z)$. In Sec. IX, they are compared with the experimental plots.

B. Equations of motion

There are three sets of equations, corresponding to three different regimes of the motion of sphere 1: no contact with the fixed sphere (hydrodynamic interactions only); pure rolling at contact with the fixed sphere; and rolling with slip at contact with the fixed sphere. The external forces, specified by Eqs. (13)–(21), and substituted into Eq. (5), result in the following motion in each of those three cases. Hydrodynamic interactions only:

$$\frac{\sin \theta}{\sin \theta_0} = \exp \left[- \int_{\xi_0}^{\xi} f(\xi') d\xi' \right], \quad (22)$$

$$U_{1z}/v_0 = [m(\xi) \cos^2 \theta - t(\xi)], \quad (23)$$

$$U_{1x}/v_0 = m(\xi) \cos \theta \sin \theta. \quad (24)$$

Pure rolling at contact:

$$\xi = \xi_m = \text{const}, \quad (25)$$

$$U_{1z}/v_0 = -r(\xi_m) \sin^2 \theta, \quad (26)$$

$$U_{1x}/v_0 = r(\xi_m) \sin \theta \cos \theta. \quad (27)$$

Rolling with slip at contact:

$$\xi = \xi_m = \text{const},$$

$$U_{1z}/v_0 = -[t(\xi_m) \sin^2 \theta - \mu_k q(\xi_m) \cos \theta \sin \theta], \quad (28)$$

$$U_{1x}/v_0 = [t(\xi_m) \cos \theta \sin \theta - \mu_k q(\xi_m) \cos^2 \theta]. \quad (29)$$

The transition from pure rolling to rolling with slip is obtained when R/P drops from μ_s to μ_k . That is, at the following angle θ :

$$\tan \theta = \tan \theta_s \equiv \mu_s / p(\xi_m). \quad (30)$$

The quantity v_0 in Eqs. (22)–(29) is the Stokes velocity:

$$v_0 = \frac{2}{9\eta} a^2 (\tilde{\rho} - \rho) g. \quad (31)$$

The functions $f(\xi)$, $m(\xi)$, $t(\xi)$, $r(\xi)$, $q(\xi)$, and $p(\xi)$ in Eqs. (22)–(30) are given in terms of components of the two-particle friction matrix, X_{11}^A , Y_{11}^A , Y_{11}^B , and Y_{11}^C [5], evaluated at the separation between sphere centers equal to $a(\xi+2)$:

$$l(\xi) = 1/X_{11}^A, \quad (32)$$

$$t(\xi) = \frac{3Y_{11}^C}{3Y_{11}^A Y_{11}^C - (Y_{11}^B)^2}, \quad (33)$$

$$m(\xi) = t(\xi) - l(\xi), \quad (34)$$

$$f(\xi) = \frac{t(\xi)}{l(\xi)(2+\xi)}, \quad (35)$$

$$q(\xi) = t(\xi) \left(1 + \frac{Y_{11}^B}{2Y_{11}^C} \right), \quad (36)$$

$$r(\xi) = \frac{3}{4Y_{11}^C + 4Y_{11}^B + 3Y_{11}^A}, \quad (37)$$

$$p(\xi) = \frac{4Y_{11}^C + 2Y_{11}^B}{4Y_{11}^C + 4Y_{11}^B + 3Y_{11}^A}. \quad (38)$$

We calculate them using our FORTRAN program, based on the Jeffrey-Onishi [5] expansion in inverse powers of the distance between particles.

The moving particle trajectories and velocities are parametrized by ξ for separation, and by θ at contact. To obtain the dependence of velocity components on vertical position z , Eqs. (23), (24), (26), (27), and (28), (29) need to be supplemented by the relation

$$z = a(2 + \xi) \cos \theta, \quad (39)$$

with θ given by Eq. (22) for separation, and with ξ given by Eq. (25) at contact. Before applying the model, we first study the experimental system and its parameters in detail, to check for consistency, to make necessary improvements, and to become aware of the model limitations.

VII. GETTING ACQUAINTED WITH THE EXPERIMENT

A. Geometry of the experimental system

The experimental cell consists of two spherical particles immersed in a very viscous fluid filling a closed cylinder (Fig. 8). The axis of the cylinder is vertical. The first ball is fixed (it can neither shift nor rotate) in such a way that its

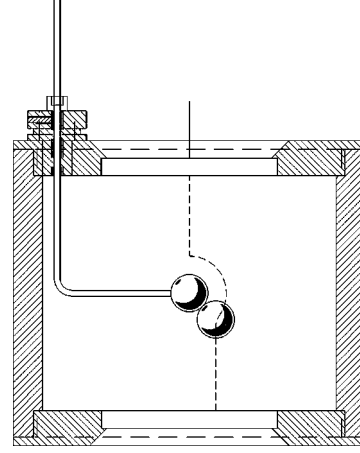


FIG. 8. The experimental cell.

center is in the middle of the cylinder. The motion of the second sphere is investigated from the moment it starts at the top wall until it stops at the bottom wall. The initial position is shifted from the axis of the cylinder by a certain distance x_0 , which changes in subsequent trials. The experimental cell presented in Fig. 8 is one of many created in the redesign process, carried out to reach high accuracy in the experiment by first investigating, and then decreasing, the side effects of the walls and of the support, and preserving the symmetry of the system at the same time.

B. Parameters and materials

The cell is a cylindrical container made of altuglas, with an inner diameter of 50.00 ± 0.01 mm and a height of 40.00 ± 0.01 mm, closed at both ends with windows made of glass of optical quality. The fixed particle is located in the center of the cell, with the help of a rod of about 1 mm in diameter (see Fig. 8). The horizontal part of the rod is about 21 mm long. The size of both particles is approximately the same, and the choice of materials is such that no magnetic effect occurs.

The moving particle is a steel ball with a mass density of about 7800 kg m^{-3} , and 6.35 ± 0.01 mm in diameter. Departure from sphericity was negligible ($0.2 \mu\text{m}$), and the arithmetic roughness R_a as indicated by the manufacturer is $0.013 \mu\text{m}$.

The fixed particle is a polyacetal sphere of 6.30 ± 0.02 mm in diameter, with a departure from sphericity estimated as $10 \mu\text{m}$. No information of roughness has been given by the manufacturer, but our scanning electron micrograph, shown in Fig. 9, gives some idea about the roughness geometry.

The fluid is the silicon oil Rhodorsyl 47V100000 (manufactured by Rhône-Poulenc) of mass density 978 kg m^{-3} and kinematic viscosity $\eta/\rho \approx 0.1 \text{ m}^2 \text{ s}^{-1}$ at 25°C . The Reynolds number of the flow due to the sedimenting ball is very small:

$$\text{Re} \approx \frac{\text{particle diameter} \times \text{maximal particle velocity}}{\text{kinematic viscosity}} \approx 6 \times 10^{-5}. \quad (40)$$

The Stokes velocity defined by Eq. (31) is about 1.5 mm/s.

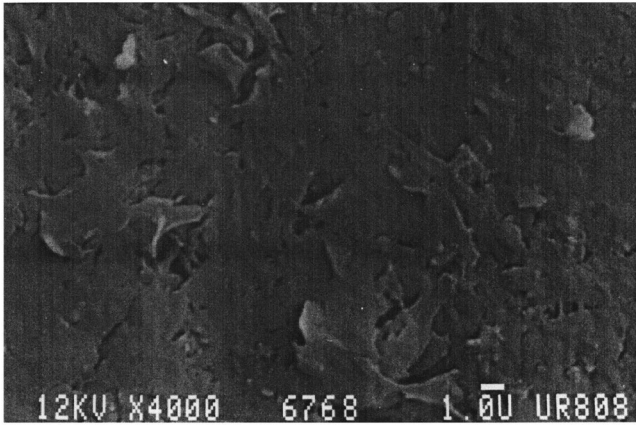


FIG. 9. Scanning electron micrograph of the fixed sphere surface.

VIII. ADJUSTMENT BETWEEN THE MODEL AND EXPERIMENT

A. Interactions with the walls and the support

Our model is valid for an infinite fluid, and therefore it does not take into account the hydrodynamic interactions with the walls. In our experimental setup this effect is important even in the central part of the container, since the ratio of the particle diameter to container height is quite large ($2a/H \approx 15\%$). According to the method of reflections [13], this parameter estimates the order of the decrease of the particle velocity due to the hydrodynamic interactions with the walls.

The question remains how to adjust the model to account for the wall effects. We will discuss this problem only very briefly—solving it needs a separate treatment.

For the contact motion, lubrication phenomena are important, and the question is how they depend on hydrodynamic interactions with the walls. In standard lubrication theory [1–5], the two-particle friction matrix elements consist of two parts. The first one depends only on the gap region, and therefore is not affected by the presence of walls. It contains terms diverging with the decreasing distance between surfaces $\xi \rightarrow 0$. The second part depends on the fluid flow everywhere, and therefore it will be modified by the presence of the walls. In the limit $\xi \rightarrow 0$ it is finite and nonvanishing.

Since in our model there is no motion along the line of centers at the contact, then the lubrication forces diverge very slowly with the decreasing distance. For small ξ the friction coefficients Y_{11}^A , Y_{11}^B , and Y_{11}^C can be approximated by [2,4,5]

$$g \ln \xi^{-1} + C + h \xi \ln \xi^{-1}. \quad (41)$$

The walls affect C , but neither g nor h [1,2,4]. For $\xi \sim 10^{-5} - 10^{-2}$ both parts $g \ln \xi^{-1} + h \xi \ln \xi^{-1}$ and C are of the same order. Therefore a modification due to the walls seems to be needed not only for separated spheres, but also for the motion at contact.

Previous experiments [10] have shown that for a single sphere sedimenting in the same cylinder, the hydrodynamic interactions with the walls cause a decrease of the vertical velocity v_z of the single particle sedimenting in the same cylinder with respect to its Stokes velocity v_0 , in such a way

that in the central part of the cylinder the ratio $v_z/v_0 \approx 0.7$, and it changes with z very slowly. This has motivated us to suppose that a modification of the constant C due to hydrodynamic interactions with the walls does not change significantly with position at the central part of the container, where the motion at contact takes place. In short, the constant C in the presence of walls can be replaced by another smaller constant C^{eff} . Since ξ does not change during the motion at contact, the term $g \ln \xi^{-1} + h \xi \ln \xi^{-1}$ does not change either. As a result, the ratio of C^{eff} to $g \ln \xi^{-1} + h \xi \ln \xi^{-1}$ is approximately constant at contact. Therefore, we might expect that at contact the interactions with the walls cause an effect similar to the decrease of the Stokes velocity.

Thus as a first approximation we make an *ad hoc* assumption that the hydrodynamic interactions between two spheres at contact can be approximated by the model presented in Sec. VI, but with the Stokes velocity (31) replaced by a smaller constant “effective Stokes velocity,” due to the hydrodynamic interaction with the walls. This way v_0 in Eqs. (23)–(29) loses its original meaning [Eq. (31)], and it becomes a parameter of the model, to be fitted from the experimental data.

The concept of an effective *constant* Stokes velocity has also been applied [9] to describe the motion at separation, driven by the hydrodynamic interactions only [Eqs. (23) and (24)]. However, such a generalization does not seem to be justified for the separating motion, when the order of magnitude of ξ changes significantly. That is, for such an increase of ξ , the ratio of $|g \ln \xi^{-1} + h \xi \ln \xi^{-1}|$ to $|C^{\text{eff}}|$ decreases. Therefore, if an effective Stokes velocity also makes sense in this case, then it is expected to change with such a significant increase of the distance between surfaces. Thus an analysis of the motion at separation becomes a complex problem. We do not address this in this paper, since our goal is to concentrate on the basic features of the motion at contact.

To make a close relation between the model and the experiment, the geometry of the experimental system has been adjusted. That is, the cell has been redesigned to preserve symmetries of the fixed sphere and the walls under reflection in the vertical plane containing the fixed sphere center and the support; and reflection in the horizontal plane containing the fixed sphere center and the support. The support (see Fig. 8) still does not preserve the symmetry. However, its influence is negligible, as it has been tested experimentally [12].

If, in addition, the initial position of the moving sphere center, the fixed sphere center, and the axis of the support are in the same plane (as has been approximately satisfied in the experiment), then the analysis of symmetries remains the same as in Secs. II B, II C, and IV A, in agreement with the nonsymmetric experimental plots in Figs. 2–4.

B. Particle size

We approximate the size of the particles by the same diameter $2a = 6.325$ mm (that is, the average of the real particle diameters, measured with the accuracy ± 0.01 mm—see Sec. VII B). This way we restrict the accuracy of the model to be no better than about 1%.

C. Container motion

Since the container moves horizontally to keep the sedimenting sphere in the laser beam, we need to discuss how it is taken into account by the model equations. The real boundary conditions for the fluid are such that there is a uniform ambient flow due to the horizontal container motion. (The ambient flow is different for various time instants. Therefore, the Stokes equations are solved for each time instant separately. This is justified because the particle and the fluid acceleration and inertia effects are negligible.) Using the linearity of the Stokes equations, we have solved an equivalent problem, with the new boundary conditions given by Eqs. (3) and (4), with a vanishing fluid flow at infinity and with the fluid velocity at the particle surface equal to the particle velocity decreased by the ambient flow (i.e., measured relative to the container). Since the container is driven horizontally in such a way that the particle horizontal position does not change, then U_{1x} in Eq. (4) has the meaning of minus the container velocity, while U_{1z} is the particle vertical velocity.

IX. INTERPRETING THE EXPERIMENTAL DATA BY THE MODEL

In this paper we present only brief estimates, which test the applicability of our model, postponing a systematic treatment for further studies. Therefore, here we restrict our analysis to a single representative trajectory at contact. The same treatment can be repeated for other trajectories.

In the model, there are four parameters to be fitted from the experiment: v_0 , the effective Stokes velocity; ξ_m , the minimal distance between particle surfaces at contact; μ_k , the kinetic friction coefficient; and μ_s , the static friction coefficient [related to θ_s , the critical angle at which slip occurs, by Eq. (30)].

Since at contact there is no motion along the line of centers, then $-U_{1z}/\sin\theta$ and $U_{1x}/\cos\theta$ are the same functions of θ . In addition, from the model equations (26)–(29) it follows that $-U_z/(\sin\theta\cos\theta)$ is a linear function of $\tan\theta$ (the same as $U_x/\cos^2\theta$). However, the slope for pure rolling, $v_0r(\xi_m)$, is significantly smaller than the slope for rolling with slip: $v_0t(\xi_m)$. An inhomogeneous term $-\mu_kv_0q(\xi_m)$ appears only for rolling with slip. Experimental results plotted in Fig. 10 confirm this model, showing a transition from pure rolling to rolling with slip, characterized not only by the slope jump, but also by a change from a smooth to a fluctuating motion.

Solid lines correspond to the least-squares linear fits [17], $a\tan\theta+b$. We get the following values of the parameters:

$$b_1 \approx -(0-2) \times 10^{-6} \text{ m/s}, \quad (42)$$

$$a_1 = v_0r(\xi_m) \approx (4.2-4.6) \times 10^{-4} \text{ m/s}, \quad (43)$$

$$b_2 = -\mu_kv_0q(\xi_m) \approx -(4-8) \times 10^{-5} \text{ m/s}, \quad (44)$$

$$a_2 = v_0t(\xi_m) \approx (7.3-7.4) \times 10^{-4} \text{ m/s}. \quad (45)$$

The error bars in Eqs. (42), (44), and (45) are larger than the least-squares fit accuracy [17]. For example, the error bar in Eq. (43) is larger than 7×10^{-6} , the corresponding least-

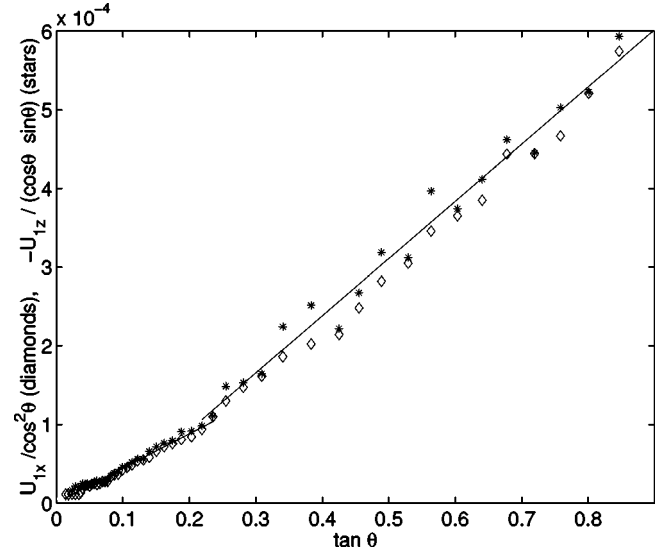


FIG. 10. Velocity at contact motion (m/s).

squares fit value. This large error has been detected while plotting the experimental data for pure rolling in the following graphs: $-U_{1z}$ versus $\sin^2\theta$, $-U_{1z}/(\sin\theta\cos\theta)$ versus $\tan\theta$, U_{1x} versus $\sin\theta\cos\theta$, and $U_{1x}/\cos^2\theta$ versus $\tan\theta$. According to Eqs. (26) and (27), all the plots should represent the same linear function $f(x)=a_1x$. However, the slopes differ from 0.00046 to 0.00042. This inaccuracy is inherent to small angles θ , at which the slope is very sensitive to small errors in determination of the relative positions of both spheres. In principle, estimates (42)–(45) allow one to look for the model parameters: the ratio $a_2/a_1 = t(\xi_m)/r(\xi_m)$ specifies ξ_m , $a_2/t(\xi_m)$ determines v_0 , and $-b_2/(v_0q(\xi_m))$ gives μ_k . In addition, from Fig. 10 we can estimate that

$$\theta_s \approx 0.23 \pm 0.02, \quad (46)$$

which allows us to use Eq. (30) to determine μ_s as the product of $\tan\theta_s$ and $p(\xi_m)$, given by Eq. (38).

Equations (43) and (45) lead to the estimation

$$a_2/a_1 = t(\xi_m)/r(\xi_m) \approx 1.58 \pm 1.72. \quad (47)$$

However, as shown in Fig. 11, the function $t(\xi)/r(\xi)$ changes very slowly with decreasing ξ . Moreover, the same figure indicates that interval (47) allows for practically any values of ξ_m .

Therefore, the error bar in Eq. (47) is too large to determine the distance between surfaces at contact, and therefore the other parameters. A brief analysis with the other parts of the motion along the same trajectory (i.e., when the spheres are separated) has shown that there is an approximate agreement between the model and the experiment in a central part of the container, which is, however, limited to very small distances between particle surfaces. However, it cannot help with the quantitative calculations—to generalize the model for larger separations, a specific procedure allowing one to calculate the effect of the walls is needed.

Nevertheless, an estimation of the model parameters can be done. First, we know that hydrodynamic interactions with the walls reduce the particle velocity. Therefore, the effective

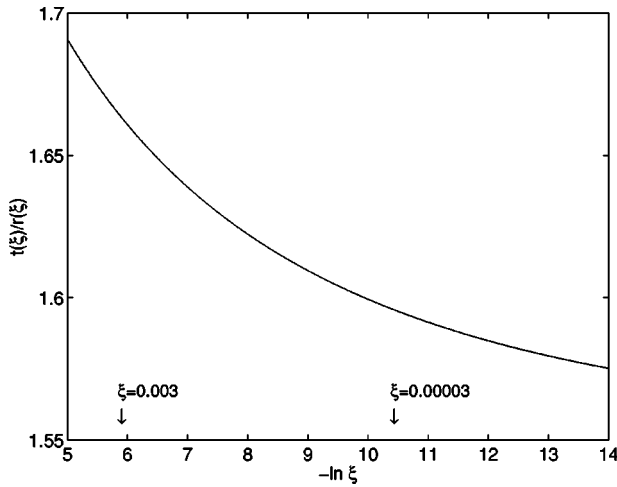


FIG. 11. Theoretical ratio of the slopes a_2/a_1 .

Stokes velocity at the contact is less than the Stokes velocity itself. Second, we assume that the distance between surfaces at contact is not larger than $10 \mu\text{m}$, an upper estimate for the roughness distance, made *ad hoc* while looking at the scanning electron micrograph (Fig. 9) of the fixed particle surface (we expect that the asperities elastically deform at contact, with a decrease of the fluid layer thickness between surfaces). Using Eqs. (43)–(45), we obtain the following estimates for the parameters of the model:

$$\xi_m = 0.00003 - -0.003 \leftrightarrow 0.1 - 10 \mu\text{m}, \quad (48)$$

$$v_0 = 1.2 - 1.5 \text{ mm/s}, \quad (49)$$

$$\mu_k = 0.09 - 0.17, \quad (50)$$

$$\mu_s = 0.13 - 0.17. \quad (51)$$

There is a large uncertainty of the resulting values of the parameters, although the vertical displacement has been measured with a very high accuracy, $\Delta z \approx 100 \text{ nm}$, and the error of the horizontal position measurement is small: $\Delta x \approx 50 \mu\text{m}$. The striking feature of the comparison between the model and the experiment, and the main result of this paper, is that the experimental results accurately confirm the

basic prediction of the model, namely, the existence of two different intervals of motion due to pure rolling and rolling with slip, and a sharp transition from one to another (Fig. 10).

X. CONCLUSIONS

Contact and hydrodynamic interactions between two spheres in a viscous fluid have been investigated experimentally, using an accurate interferometric technique. A simple physical model of these interactions between very close spheres has been constructed. It is based on a plain combination of the standard hydrodynamic forces on smooth spheres at a finite small distance ξ_m , and the classical solid friction forces for rough particles touching each other. The model accounts for the symmetry breaking of the experimental velocities and trajectories. It contains corrections for the hydrodynamic interactions between the walls and the particles at contact.

The existence of two different intervals of motion, pure rolling and rolling with slip, and a sharp transition between them, was first predicted by the model, and next confirmed experimentally (Fig. 10). The high accuracy of this verification is striking, considering the simplicity of the model.

However, the comparison with the experiment is still not sufficient to determine the values of the physical parameters of the model precisely. That is, the theoretical fit is not sensitive enough to a change of the distance between surfaces.

The distance between surfaces at contact $\xi_a \approx 0.1 - 10 \mu\text{m}$ is smaller than the upper estimate of the roughness of the fixed sphere. The hydrodynamic interactions with the walls result in an effective Stokes velocity reduced by less than 25% with respect to the Stokes velocity in an infinite fluid. The kinetic friction coefficient is given as $\mu_k \approx 0.09 - 0.13$. The critical angle θ_s between pure rolling and rolling with slip determines the static friction coefficient ($\mu_s \approx 0.13 - 0.17$). Both kinetic and static coefficients agree with the typical values for lubricated metal-nonmetal contacts [14].

ACKNOWLEDGMENT

M.L.E.-J. thanks the French Ministry of Research and Education for supporting her stay at ESPCI in Paris.

-
- [1] D. J. Jeffrey, in *Sedimentation of Small Particles in a Viscous Fluid*, edited by E. M. Tory (WIT Press Computational Mechanics Publications, Southampton, 1996).
- [2] S. Kim and S. J. Karilla, *Microhydrodynamics: Principles and Selected Applications* (Butterworth-Heinemann, Boston, 1991).
- [3] D. J. Jeffrey, *Mathematika* **29**, 58 (1982).
- [4] D. J. Jeffrey and Y. Onishi, *Z. Angew. Math. Phys.* **35**, 634 (1984).
- [5] D. J. Jeffrey and Y. Onishi, *J. Fluid Mech.* **139**, 261 (1984).
- [6] M. Tabatabaian and R. G. Cox, *Int. J. Multiphase Flow* **17**, 395 (1991).
- [7] R. H. Davis, *Phys. Fluids A* **4**, 2607 (1992).
- [8] F. R. da Cunha and E. J. Hinch, *J. Fluid Mech.* **309**, 211 (1996).
- [9] S. Zeng, E. T. Kerns, and R. H. Davis, *Phys. Fluids* **8**, 1389 (1996).
- [10] N. Lecoq, F. Feuillebois, N. Anthore, R. Anthore, F. Bostel, and C. Petipas, *Phys. Fluids A* **5**, 3 (1993).
- [11] E. Lecoq, Engineering degree report, Conservatoire National des Arts et Metiers, Paris, 1997 (unpublished) (in French).
- [12] K. Masmoudi, Ph.D. thesis, Universite de Rouen, 1998.
- [13] J. Happel and H. Brenner, *Low Reynolds Number Hydrodynamics* (McGraw-Hill, New York, 1963).

- [14] S. H. Crandall, N. C. Dahl, and T. J. Lardner, *An Introduction to the Mechanics of Solids* (McGraw-Hill, New York, 1978).
- [15] K. L. Johnson, *Contact Mechanics* (Cambridge University Press, Cambridge, 1985).
- [16] F. P. Bowden and D. Tabor, *The Friction and Lubrication of Solids* (Clarendon, Oxford, 1950, Vol. I, 1964, Vol. II).
- [17] P. R. Bevington, *Data Reduction and Error Analysis for the Physical Sciences* (McGraw-Hill, New York, 1969).